

Stochasticity Modeling in Memristors

Rawan Naous, *Student Member, IEEE*, Maruan Al-Shedivat, *Student Member, IEEE*,
and Khaled Nabil Salama, *Senior Member, IEEE*

Abstract—Diverse models have been proposed over the past years to explain the exhibiting behavior of memristors, the fourth fundamental circuit element. The models varied in complexity ranging from a description of physical mechanisms to a more generalized mathematical modeling. Nonetheless, stochasticity, a widespread observed phenomenon, has been immensely overlooked from the modeling perspective. This inherent variability within the operation of the memristor is a vital feature for the integration of this nonlinear device into the stochastic electronics realm of study. In this paper, experimentally observed innate stochasticity is modeled in a circuit compatible format. The model proposed is generic and could be incorporated into variants of threshold-based memristor models in which apparent variations in the output hysteresis convey the switching threshold shift. Further application as a noise injection alternative paves the way for novel approaches in the fields of neuromorphic engineering circuits design. On the other hand, extra caution needs to be paid to variability intolerant digital designs based on nondeterministic memristor logic.

Index Terms—Memristor, memristor model, neuromorphics, stochasticity, stochastic electronics, threshold-based devices.

I. INTRODUCTION

THE term stochastic electronics has been coined lately with the introduction of the non-deterministic behavior of circuit elements [1]. It is a newly established field of study that has set the standards for incorporating the intrinsic variability within the emerging devices into the circuit design and simulation phases of the system process [2]. Stochastic electronics are on the rise at a fast pace to compete with traditional technologies in providing alternative solutions coping with the nanoscaling and extensive integration in what is addressed to as beyond Moore's law [3]. It is the rising norm rather than the sheer trend nowadays to have systems that exhibit a certain level of variability in its operation in an attempt to be the best fit for the brain scale mimicking behavior [4]. It allows for the accounting of this random behavior in error-tolerant systems to aid in achieving great potentials in computation, processing and storage in a model fitting to the biologically plausible systems. Particular high profile candidates are novel non-volatile technologies, such as spin transfer torque random access memory [5], phase change

memory (PCM) [6], and conductive bridge RAM (CBRAM) [7]. The memristor is central to this operation as well, and it has been considered in many applications to hold a close resemblance to the basic building blocks of the human brain architectures. In applications with biologically inspired stochastic computation [7], [8] and neuromorphic systems [9]–[13], as synapses [14], and neurons [15]–[18].

Memristors are typically composed of two conducting metal electrodes separated by an insulating active layer that allows resistive switching under an induced electrical excitation [20], [21]. It is simply a resistor with memory, where the value of the resistance is retained even after the removal of the acting potential. Threshold-less device models exhibit a continuous change of resistance upon application of input stimuli [22]. However, for threshold based devices, the change is only initiated once a set threshold is reached [23]. The switching or shift from a low to high resistance level and vice versa is initiated once the input across the two terminals reaches a certain inherently set value. Nonetheless, in any of the memristor types, the internal ionic and chemical processes in these devices depend mainly on the underlying material characteristics. It is an overall interaction progression that involves interfacial features of the metals along with the diffusion properties of the insulating material [24], [25]. This complex entanglement predominantly controls the overall operation and switching mechanism of the memristor. Several models have been proposed to describe this behavioral process. Propositions varied in complexity to either precisely meet fabricated devices and physical dynamics [22], [26], [27] or as a practical fit with a more abstract mathematical formulation of a generalized switching process [23], [28]–[31]. Further to the deterministic behavior of the memristor, the variants of the underlying material composition and interactions impose a new domain of operation. A stochastic outcome stemming from the switching characteristics and the kinetics of the ionic and chemical reactions is observed but immensely overlooked in the circuit modeling process. Inducing the stochasticity feature into the circuit models of the memristor paves the way for capturing actual device behavior while overlying the physical variability origins. It further allows for unconventional applications and testing platforms.

In this paper, a circuit compatible model is proposed comprising the switching point variability applied to threshold-based models of memristors. It is an agile formulation that can be easily integrated with any of the established models to induce stochasticity while preserving the individual kinetics. The experimental observations and corresponding explanations of the stochasticity among the emergent nonvolatile memories are addressed and introduced in Section II. It acutely stresses on the variability of the physical medium and its consequent operation influence. Particular elaboration on the origins and impact of the

Manuscript received April 3, 2015; revised October 1, 2015; accepted October 4, 2015. Date of publication October 26, 2015; date of current version January 6, 2016. This work was supported by the King Abdullah University of Science and Technology, Saudi Arabia. The review of this paper was arranged by Associate Editor S. Pontarelli.

R. Naous and K. N. Salama are with the Computer, Electrical, and Mathematical Sciences and Engineering Division, King Abdullah University of Science and Technology, Thuwal 23955, Saudi Arabia (e-mail: rawan.naous@kaust.edu.sa; khaled.salama@kaust.edu.sa).

M. Al-Shedivat is with the Machine Learning Department, Carnegie Mellon University, Pittsburgh, PA 15213 USA (e-mail: Maruan.Shedivat@kaust.edu.sa).

Color versions of one or more of the figures in this paper are available online at <http://ieeexplore.ieee.org>.

Digital Object Identifier 10.1109/TNANO.2015.2493960

switching variability is further addressed with emphasis on the model proposed and its subsequent verification. Section III covers the current and voltage threshold models that are extended to account for variability with output results focusing on the variation of the typical hysteresis behavior. Design applications are investigated in Section IV where analog and digital counterparts provide a contrasting view of the stochastic conditions. The conclusion holds the overall summary of the proposed model and the various resulting operations.

II. EMERGING TECHNOLOGIES AND STOCHASTICITY

The notion of stochasticity in the operation of memristors is not a novel feature perceived in a unique device, but rather a continuum of advances for studies addressing the internal switching phenomena and its underlying probabilistic nature [32], [33]. Intrinsic variability has been perceived across a range of emerging nonvolatile memory technologies such as PCM [6], [34], resistive random access memory [35], [36], electrochemical metallization memory [37], CBRAM [7], and among oxide-based memristive material [32], [33], [38]. Despite the differences in the above technologies, the common ground agreement among this variant of devices is essentially the consensus on the role of the internal physical characteristics. To that end, stochasticity is mainly attributed to the underlying constituting elements and the resulting conducting filament (CF) formation process [20], [24].

Supporting mathematical formulations are provided to explain the origins of the perceived stochasticity with varying levels of investigation of the underlying physical medium. On one extent, a fine behavioral perspective on the ionic process and the vacancy generation consider them as the primary factors in the complex formation of the CFs between the two metal electrodes of the device [35], [39]. A detailed model of the switching of the metal oxides builds upon a probabilistic migration/recombination of ions and consequently the closing gap between the filaments and the metal layer. Fig. 1 illustrates the CFs variation along with the gap formation with the corresponding motion dynamics of the ions. This gap width variation was modeled with a Gaussian distribution to account for the randomness of the ions propagation along the complete dimension of the device. A circuit compatible model for this innate stochasticity mainly apparent in ReRAMs was presented in [40]. It conveys the underlying mechanisms of the ions with added stochasticity, providing a set kinetics of the device behavior.

On the other extreme, particularly in [7] and [41] switching was seen to be variable with attributes originating from the probabilistic formation/rupture of the CF. This status arises due to the non-deterministic residue that remains after the rupture of the filament in the reset process. A resultant output of this inherent variability is the variation of the high and low resistance states, where the values follow a log-normal distribution as fitted to the experimental measurements under weak programming conditions. That is where the subthreshold voltage application will have a vital effect on the resultant behavior. This analytical model captures the eventual response of the device and its corresponding resistance states, R_{on} and R_{off} , respectively.

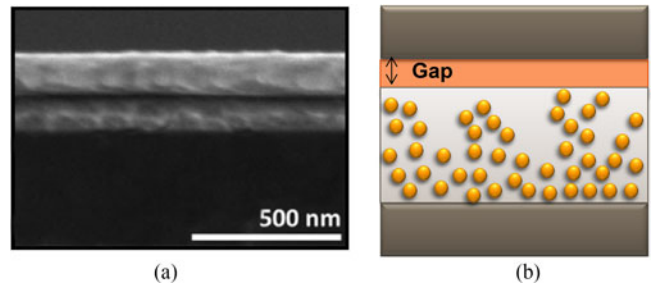


Fig. 1. *CFs-Gap Variation*. (a) Memristor microscopy (reprinted with permission from [19]). (b) Internal ionic migration and CF formation with the resulting gap separation that controls the switching operation.

Further quantifying models that abstract the switching process into a statistical event are prominently discussed in [32] and [42]. They primarily build on experimental data acquisition and consequent outcome fitting to a statistical distribution. The conducted experiments composed of applying an external stimulus to the terminals of the memristor and recording the time it required for the device to switch. For a particular device, the experiments were repeated several times for every input pulse. In each trial, once the memristor switches to the ON/OFF state, the time since the application of the input pulse is recorded, and the device is then reset back to its initial OFF/ON state. A distribution of values was depicted for the wait times for a particular input voltage. The experimental values were fitted into two main distributions, the Poisson [32], and the log-normal distribution [42]. The implication of the wait time distributions on the device operation is a probabilistic switching behavior. The threshold voltage is no longer fixed, but rather varies as a function of the amplitude and the temporal applicability of the input bias. The switching mechanism, the physical attributions, and the mathematical formulations of this particular mode of stochasticity are further illustrated in the following sections.

A. Stochasticity Distributions

The model presented in [32] builds on experimental data extraction for amorphous silicon (a-Si) memristors that yielded a Poisson-like switching process. Whereas experiments for a titanium dioxide (TiO_2) reported in [42] resulted in a log-normal distribution. Each of these models had its own set of equations and physical attributions to the source of variability.

1) *Poisson-Like Switching*: The main assumption within this model relied on the concept of a single or dominant CF formation to trigger the switching to the ON state. The formation process is based on the hopping of the metal particles, which are positively charged, into the trapping sites within the a-Si layer. It is a step-by-step chain growing process leading eventually to the complete filament structure [32], [43]. A conducting path is thus formed through the chain of metal particles and comprising the mechanism behind the conduction and consequently the resistance change.

This bias-dependent switching rate originates from the thermally activated process of the hopping for the metal particles.

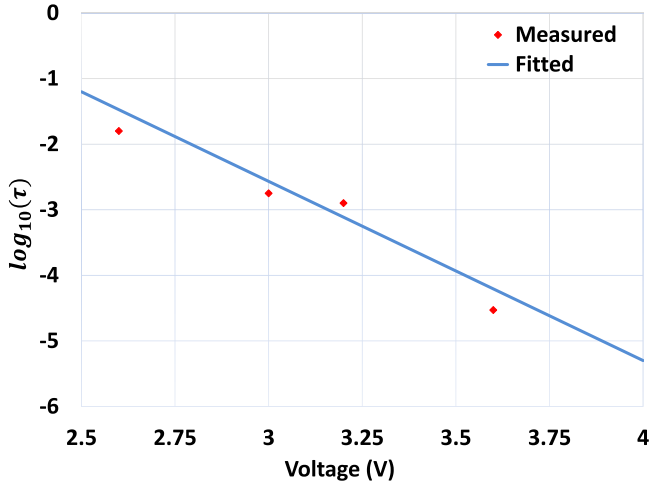


Fig. 2. *Stochastic Parameter τ fitting.* Linear fitting for the wait time in relation to the input voltage. Experimental fitting based on the data provided by Jo *et al.* [32]. The fitting parameters are α_0 and ϵ as depicted in equation (5).

The activation energy (E'_a) is bias-dependent and consequently, is the hopping rate (Γ) that is determined according to

$$\Gamma = \frac{1}{\tau} = \nu e^{-E'_a(V)/k_B T} \quad (1)$$

where ν is the attempt frequency for the particle hopping, k_B is the Boltzmann's constant, and T is the absolute temperature. With the application of an input bias, the activation energy is lowered which results in a variation in the waiting times and switching rates, respectively.

An exponential relationship is thus formulated between the characteristic wait time of the device and the applied input bias as shown in equation (2). This model formulates a simple relation between the switching probability and its sole dependence on the time and amplitude of the voltage applied to the terminals of the device. That is with a higher level of voltage; the switching is expected to occur at an earlier time compared to lower levels

$$\tau = \tau_0 e^{-\frac{V}{V_0}}. \quad (2)$$

τ_0 and V_0 are considered as fitting parameters that are a characteristic of the device and modeled in equations (3) and (4), respectively. Explanation of the physical origins of these parameters is provided in the supporting information for [32]

$$\tau_0 = 1/\nu e^{E_a/k_B T} \quad (3)$$

$$V_0 = 2nk_B T/e. \quad (4)$$

E_a is the activation energy at zero bias. It has a linear relationship with the voltage dependent activation energy, $E_a = E'_a(V) + eV/2n$. Where e stands for the electron charge, V is the input bias, and n corresponds to the number of trapping sites within the device. Experimentally, within the logarithmic scale, a linear relation was fitted according to equation (5) and depicted in Fig. 2

$$\log_{10}(\tau) = \alpha_0 V + \epsilon \quad (5)$$

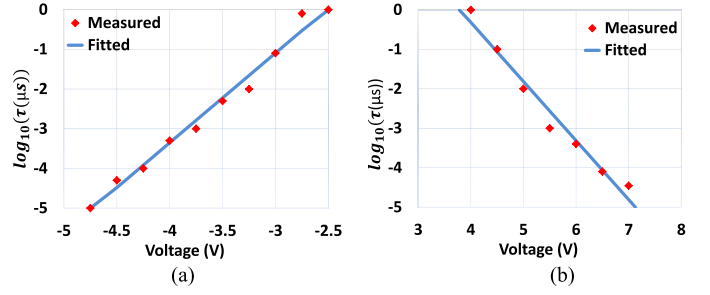


Fig. 3. *Log-normal median switching time.* (a) The exponential fitting for the measured times with respect to the input voltage for the ON switching case. (b) OFF switching case.

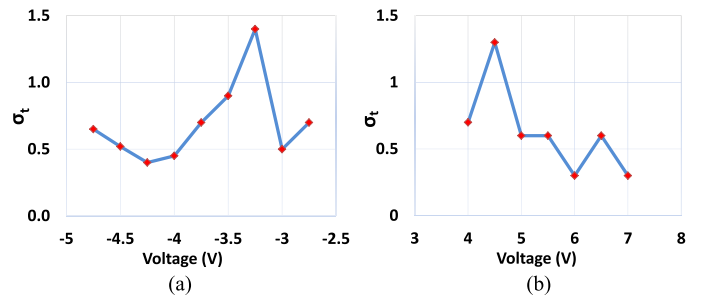


Fig. 4. *Log-normal sigma.* (a) The experimental sigma values represent orders of magnitude for a given threshold (measured in μs) extracted for the ON switching case. (b) OFF switching case.

where α_0 and ϵ are fitting parameters whose values are set according to the memristor model used. Based on the physical attributions and the relationships formulated for the underlying parameters, the switching process was considered stochastic and following a Poisson process. The conducting mechanism described earlier, in terms of the individual metal particles hopping into the trapping sites, fits into this model of a summation of independent events leading to the exponential distribution of the switching wait times. At a certain point in time t , the probability of occurrence of a switching event within an infinitesimal interval Δt is depicted in

$$P(t) = \frac{\Delta t}{\tau} e^{-t/\tau}. \quad (6)$$

This added feature paves the way for a control condition with respect to the output behavior needed. Although the individual switching points are random at instants of time, in general they exhibit a mean activity following a Poisson process.

2) *Log-normal Distribution:* An alternative statistical fitting to the switching behavior was observed in [42]. The experiments were conducted on a titanium dioxide device in a similar fashion to the above-described model. However, the switching times were mapped into a log-normal distribution rather than a Poisson. Furthermore, in contrast to the first model, the stochasticity conditions were tested for the ON and OFF switching. The exponential dependence on the input bias was apparent as well, although with a different set of fitting parameters. Fig. 3(a) and (b) depicts the fitting performed for the characteristic or median wait time τ for the ON and OFF switching cases, respectively.

TABLE I
FITTING PARAMETERS FOR THE CHARACTERISTIC WAIT TIME

| | Poisson | Log-normal (ON) | Log-normal (OFF) |
|------------------------------|---------|-----------------|------------------|
| $\alpha_0((s \cdot V)^{-1})$ | -2.67 | 2.26 | -1.49 |
| $\epsilon(s^{-1})$ | 5.43 | 5.69 | 5.67 |

The switching mechanism in this type of device is primarily based on electron tunneling through an insulating gap. The application of an input voltage or current will modify the width of this gap and the device resistance accordingly [44]. A positive bias will lead to an increase in the gap width as the oxygen vacancies, which are positively charged, are repelled towards the conducting channel. Thus leading to a higher resistance or the OFF switching. On the other hand, a negative bias will cause the vacancies to move away from the channel. It reduces by that the gap width and device resistance; leading to the ON state switching. The origin of the stochasticity perceived in this model is the attributed to density fluctuations of the distributions of the drifting vacancies/dopants. In other words, statistical variations in the vacancy concentrations rather than a smooth dispersion are the primary source of variability leading to the log-normal switching process depicted in

$$F(t_{\text{switch}}, \tau, \sigma_t) = \frac{1}{2} \operatorname{erfc} \left[-\frac{\ln(t_{\text{switch}}/\tau)}{\sqrt{2}\sigma_t} \right] \quad (7)$$

where F stands for the cumulative distribution function for the log-normal distribution, t_{switch} corresponds to the cumulative time, and erfc is the complementary error function. The distribution is characterized by its median time to switch τ and the standard distribution σ_t . As illustrated earlier, τ was calculated based on equation (5) by setting the corresponding values of α_0 and ϵ . Table I shows the values for the fitting parameters according to the reported distribution and ON or OFF switching. On the other hand, from the experimental data (Fig. 4) there was no clear relation and a very weak dependence between σ_t and the applied voltage. Thus reported hard values and interpolation was required to have the corresponding fitting. According to [45] the switching probability for a Δt is given by

$$P(t) = \frac{\Delta t}{\text{mean}} = \frac{\Delta t}{\tau} e^{-\sigma^2/2} \quad (8)$$

where τ is considered the median in the log-normal distribution, whereas the mean (μ) is $\mu = \tau e^{\sigma^2/2}$.

The chosen setting, the distributions in particular, depends on the speed and mechanism of the switching operation. Moreover, within the realm of a single model, the range of values used for these parameters dictates the operation region across time of the corresponding memristor. As illustrated from equation (6), infinitesimally small values of τ leads to almost abrupt switching, whereas with larger values of τ the operation reverts back to its original dynamics.

The general equations signifying the conductance change over time are summarized in the following two

functions [22], [46]

$$\begin{cases} u(t) = g(w, s, t)s(t), \\ \frac{dw}{dt} = f(w, s, t), \end{cases} \quad (9)$$

where the parameters $s(t)$ and $u(t)$ are the corresponding input and output functions, respectively. They form the I - V relation for the memristor depending on whether the device is a voltage or current driven. Similarly, the function $g()$ represents the mem-conductance or memresistance according to the set parameters. The liberty in the behavioral modeling of the device is mainly captured within the formulation of the state derivative dw . On the other hand, a general incorporation of the added stochasticity is modeled as a function setting for the threshold and passed over to the state function w . It could be easily mapped into any of the threshold based functions where the switching location is the sole parameter affected with stochasticity while preserving the kinetics of the original models. Equation (10) reflects the variability of the threshold voltage with the incorporation of the stochastic term

$$dV_T = \underbrace{\alpha \theta(V_{T_o} - V_T) dt}_{\text{deterministic term}} + \underbrace{(|V| - \Delta V - V_{T_o}) dN(\tau)}_{\text{stochastic term}}. \quad (10)$$

The functions $\theta()$ and $N(\tau)$ are the step function and the Poissonian/log-normal process, respectively. V is the input voltage, δV stands for the infinitesimal change for the voltage to allow for the setting of the threshold voltage accordingly, α is a fitting parameter set according to the model used, and V_{T_o} is the almost deterministic threshold voltage of the device. That is, the voltage at which the switching becomes almost certain following the switching probabilities described in equations (6) and (8). Thus, at every instant of time the switching voltage has a probability of changing according to the stochastic process defined in $N(\tau)$.

B. Verilog-A Model

The endorsed stochasticity condition was modeled in a circuit compatible model using Verilog-A. It allows for behavioral simulation and testing in an easy integration with SPICE modules. It provides an easy integration of the stochasticity conditions building solely on the statistical characteristics of the switching process and overlying the underlying physical attributions. The central idea of variability relies upon the shift in the switching point for the memristor as its particular value depends on the probability calculated at every time step. Cumulatively the complete operation follows a Poisson/log-normal distribution, whereas the corresponding switching events are random in time and decided upon at every instant as depicted in Algorithm 1. While the *Verilog-A* code is included in the appendix of the manuscript.

That is at each instant of time, the switching might arbitrary occur or not. The logic for the *Verilog-A* code is illustrated in the following algorithm. The main concept lies in picking a sample from a uniform random distribution and comparing it to the probability of switching calculated at each point in time. In case

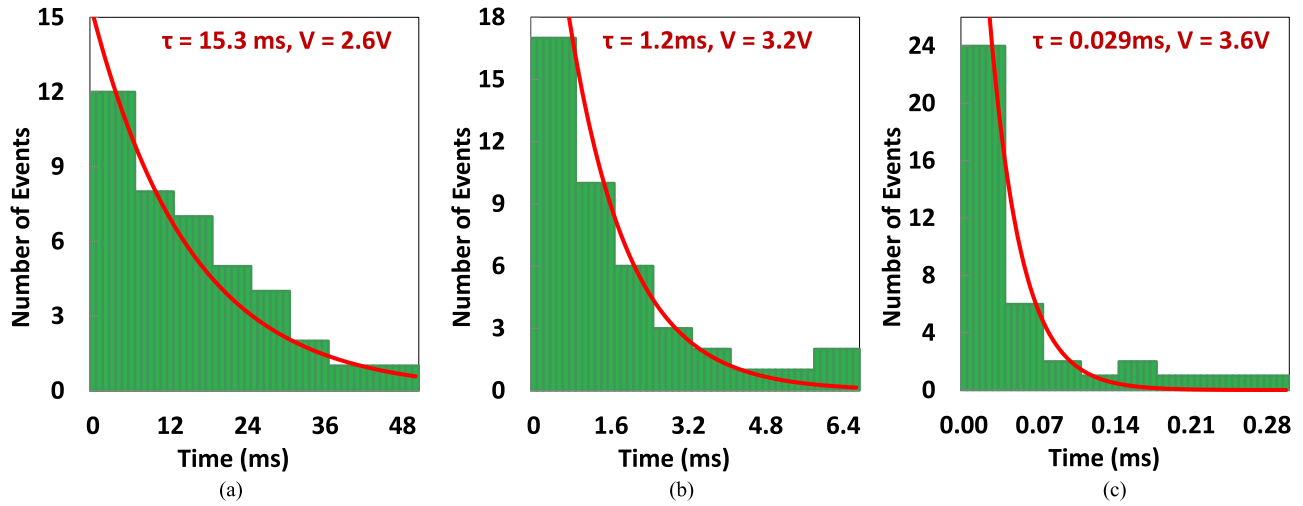


Fig. 5. *Experimental Poisson.* (a) Data fitting for the switching times reported in [32] for varying input voltage pulse of 2.6, (b) 3.2 and (c) 3.6 V, respectively. The characteristic switching times extracted increased with the smaller input voltage. The Distributions were fitted with the characteristics parameters accordingly.

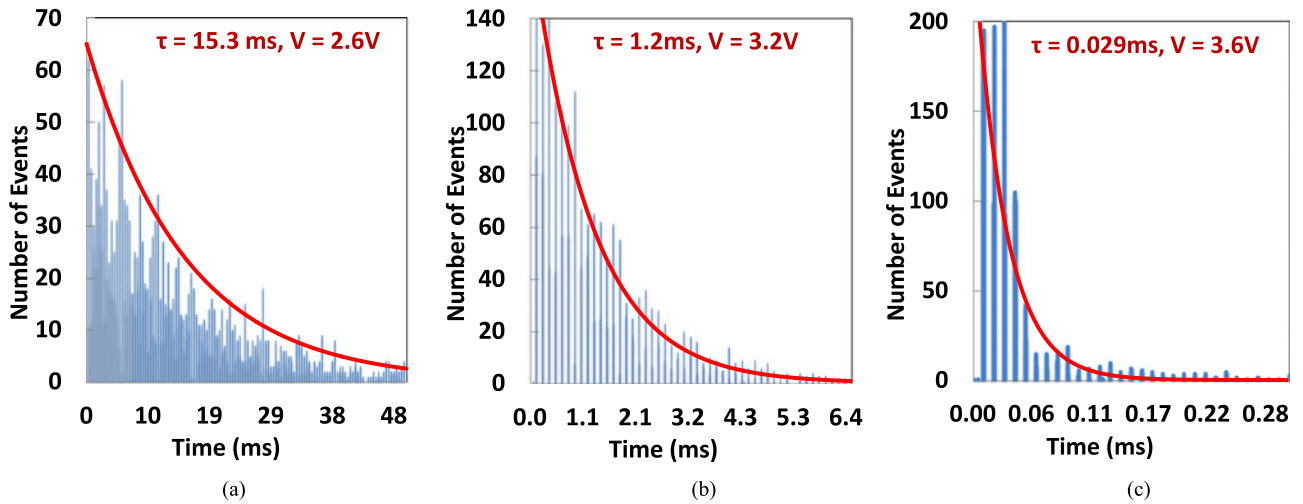


Fig. 6. *Simulation Data.* (a) The simulated model incorporating the variability of the threshold voltage for the same set of input voltages for the reported measurements. The voltage pulses of 2.6, (b) 3.2 and (c) 3.6 V were applied and mapped into the fitted Poisson.

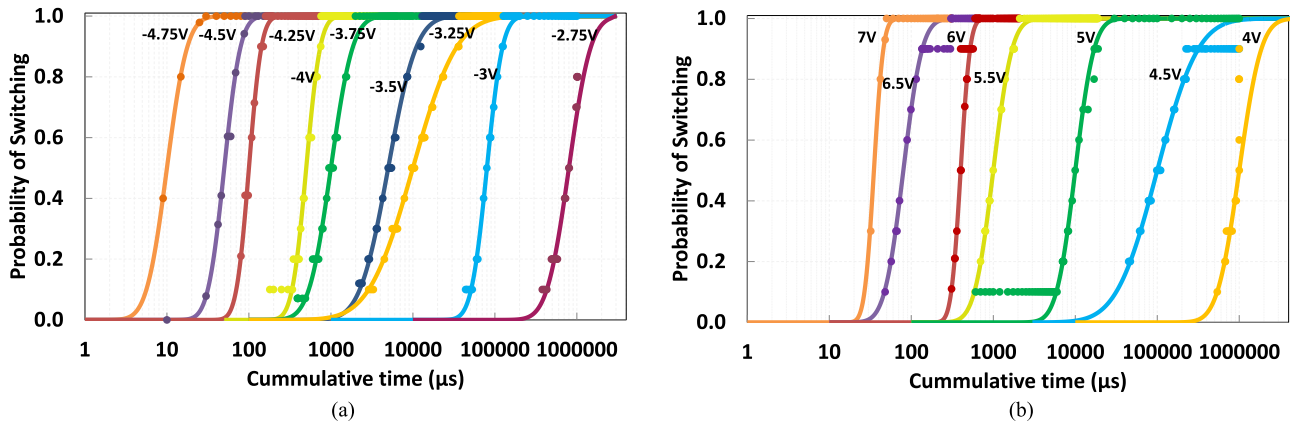


Fig. 7. *Log-normal Experimental fitting.* The cumulative switching times distribution fitting of the experimental data reported in [42]. (a) The ON switching distribution and (b) OFF switching.

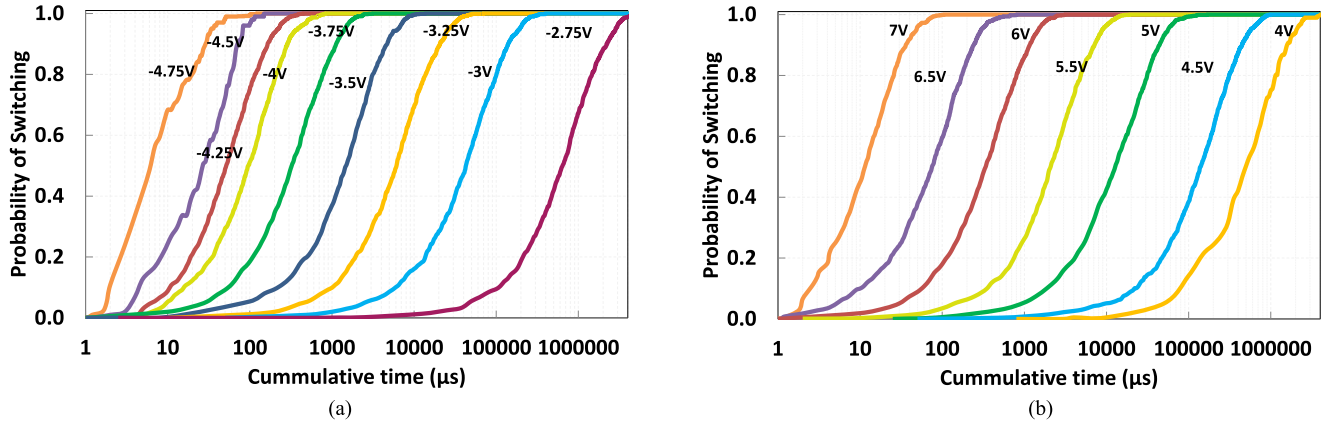


Fig. 8. *Log-normal Simulations*. Stochastic model simulations for the different voltage pulse inputs with the cumulative switching times for the (a) ON switching and (b) OFF switching cases.

Algorithm 1: Threshold voltage Statistical Variation

```

Choose the switching distribution;
Calculate the characteristic parameters;
for every time instant do
    Calculate the corresponding probability  $P$ ;
    Sample from a uniform random distribution  $R$ ;
    Compare;
    if  $P \geq R$  then
        threshold voltage is set to the current input
        voltage;
    else
        The threshold voltage is not changed;
Pass on the threshold voltage

```

the calculated probability is greater than the chosen sample, the threshold voltage takes the value of the instantaneous voltage, and the switching occurs accordingly. Otherwise, the threshold voltage remains at the almost deterministic case set for the particular device. This stochasticity modeling is added to any of the readily established memristor models. The main idea is to have the threshold conditions variable at instants of time and provide them as an input to the corresponding switching criteria.

C. Model Verification

The generalized stochastic model could be induced in simulation to different memristor formulations emphasizing on the non-deterministic behavior of the output hysteresis. A further verification in terms of the mapping of the model to the experimental measurements of stochastic devices is illustrated in this section. It primarily focuses on the switching mechanism and its time–amplitude relationship. Where the average switching times would decrease with the higher input voltage levels applied. It narrows further into the switching events of a particular input voltage set. It is with increasing probability, $P(t)$ increasing towards 1 that the device will switch when the time of the application of the input pulse is larger than the switching time constant. In other words, when t exceeds τ . It aims to pro-

vide a distribution fitting to the characteristics of the principle device-extracted data.

1) *Poisson Fitting*: The basis of the proposed model is rooted back to the quantification process applied to the abstract switching events of the memristor. In [32] a Poisson-like process was experimentally extracted from the behavior of fabricated devices. In this section, the extent to which the Verilog-A model acutely fits into the distribution is measured through the application of a set of voltage pulses with different amplitudes. The applied input voltages are chosen to match the reported values for the measurements. The process of measurement is set for each particular voltage. For every trial, a pulse is applied, the time at which the switching occurs is recorded, the device is reset back to its original state, and then another trial starts. For simulation, a Python script was used to generate the SPICE netlist and extract the resulting switching times. The algorithm was run over for ten thousand trials for each voltage input.

The exact value of the average waiting time is mainly dependent on the level of applied voltage. As illustrated earlier, the amplitude level increase reduces drastically the time for the device to switch. Fig 5(a) shows the experimental data reported in [32] and its corresponding fitting to the Poisson switching process for three different voltage pulses. Whereas Fig 6(b) represents the simulated results, for the same applied set of applied voltage as the experimental ones, with the application of the threshold variation technique within the memristor model. As depicted in the graphs, the simulations match the measurements and the time constants reported in the experimental data. The higher the voltage applied, the switching times for the device gets more concentrated towards the origin.

2) *Log-Normal Fitting*: The Verilog-A model incorporated the log-normal distribution aside to the Poisson, with an option to choose the type of statistical variability to be induced. The verification of this particular distribution is based on the cumulative switching times, and their corresponding probability, that were extracted from the experimental measurements in [42]. As depicted in Fig. 7(a) and (b) the ON and OFF cumulative switching probabilities are fit to the log-normal sigmoid shaped function. Similarly to the simulation trials illustrated in the earlier section, the trails were run for ten thousand times and

the switching times were recorded. The switching probability was then calculated by dividing the number of events, for each switching time, over the total number of trials. Fig. 8(a) and (b) shows the corresponding simulation results for the ON and OFF switching, respectively. A clear dependence on the voltage is apparent in both cases of switching. The probability of switching becomes higher much faster with higher input voltages. The time constants also follow the same behavior to the experimental data where longer times are required to switch for smaller voltages. However, there is a minor shift in terms of the time constants and the shaping parameters from the experimental data due to the dual approximation that was proposed in [42] for τ and σ_t . Nonetheless, the overall behavior of the system is captured by the simulation model using the fitting parameters from Table I.

III. MEMRISTOR MODELS

The dynamics of the memristor device have been under thorough investigation aside to modeling attempts to adequately capture its non-linear behavior. Models proposed along several domains have set standards in terms of complexity, accuracy and practicality in simulation and circuit design [47]–[55]. In general, charge or flux controlled operations are the two variants imposing a dependence on the history of the applied current or voltage respectively across the terminals of this nano-scale structure. The considered models in this paper are variants of voltage and current driven into with emphasis on varying abstraction and general fitting of the stochasticity effect. It starts with an abstract model of voltage switching and considers as a well a model fit for neuromorphic applications. Furthermore, the original model presented by Pickett, mainly a current driven model, is investigated and padded with stochasticity effects. Covering by that a broad spectrum of models and a corresponding fit for applications.

A. Bipolar Memristors With Threshold

In this model [28], [56], [57], the authors are introducing a general model of the circuit element exhibiting a memory characteristic with a rate of change related to the applied voltage. In its deterministic version, no response is perceived below the threshold. Its switching state starts to increase at a certain rate β that acts as the slope of the internal dynamics of the memristor. Fig. 9(a) depicts the general shaping of the threshold based memristive device. Its behavior is modeled by a linear I - V relationship and a shaping function describing the internal process and the sensitivity to the limiting parameters as illustrated in

$$I = X^{-1}V_M \quad (11)$$

$$\frac{dX}{dt} = f(V_M)[\theta(V_M)\theta(R_{\text{off}} - X) + \theta(-V_M)\theta(X - R_{\text{on}})] \quad (12)$$

$$\begin{cases} f(V_M) = \beta V_M - 0.5\beta[|V_M + V_t| - |V_M - V_t|], \\ dV_T = \underbrace{\alpha\theta(V_{T_o} - V_T)dt}_{\text{deterministic term}} + \underbrace{(|V| - \Delta V - V_{T_o})dN(\tau)}_{\text{stochastic term}}. \end{cases} \quad (13)$$

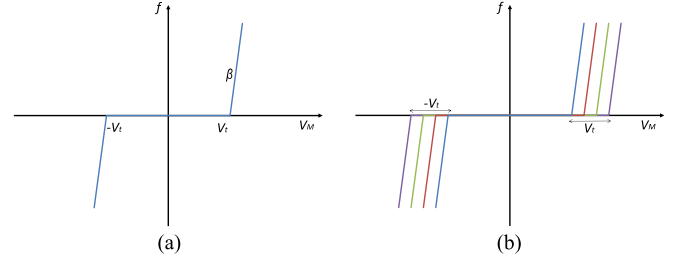


Fig. 9. *Model Dynamics.* (a) Internal dynamics of the voltage controlled model. (b) Stochastic dynamics. resultant variation in the threshold voltage with the mere shift in the location of switching and preservation of the original function kinetics.

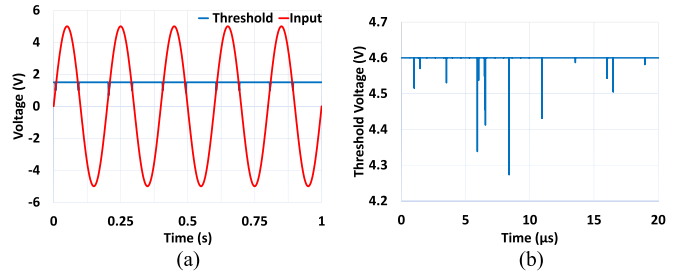


Fig. 10. *Variability of the threshold voltage.* (a) Response to a sinusoidal input voltage showing the larger variation particularly at closer voltages to the original threshold. (b) A finer resolution of the threshold variation.

The memristance is reflected within the state variable X and is limited by the upper and lower boundaries R_{off} and R_{on} . The function θ is the step function responsible for enforcing this constraint. Incorporating the variability into this model follows a straightforward approach where the threshold voltage V_t is varied in a way abiding by the stochasticity measures explained earlier and depicted in (13). It allows for sub-threshold switching in a non-deterministic fashion where the value of the point of switching is related to the input voltage application time and amplitude. The direct implication to the inherent stochasticity is a variable threshold voltage that is particularly susceptible to voltages close to its original fixed value where a higher probability of switching occurs. The variation of the threshold is apparent in Fig. 10(b) that depicts the variation in response to the input voltage application. This behavior is reflected in the shaping function fluctuation at the point of switching while preserving the kinetics of the system as shown in Fig. 9. Moreover, the resultant output for this stochastic behavior is apparent in the hysteresis depicting the relation between the voltage and current respectively. Instead of having a single response for a sinusoidal input, the output is tainted with added inner hysteresis encapsulated within the outer limits set by the deterministic threshold voltage. Fig. 11(a) shows the original graph aside to the stochastic output in Fig. 11(b).

B. Analytical Memristor Model

A slower version of memristors, particularly suitable for neuromorphic applications, is presented in the model in [58]. Several fabricated devices have been aligned into the equations of

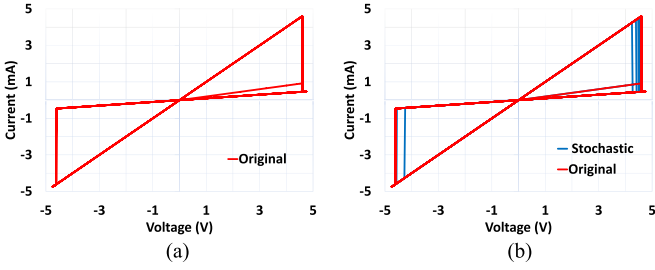


Fig. 11. *Stochastic Hysteresis Output.* (a) Deterministic output of the model with the parameters specified in [57]. (b) The stochastic output with the outer hysteresis setting confining the subthreshold stochastic switching.

the proposed model based on a fine tuning of the fitting parameters. It is set to a generalized form that is characterized by a nonlinear I - V relationship as shown in (14), where the parameters a_1 and a_2 are used as amplitude parameters to account for the conductivity of the different device structures along with polarity of the applied input. Moreover, a control factor is also included where b calibrates the intensity of the threshold in relation to the voltage amplitude

$$I(t) = \begin{cases} a_1 x(t) \sinh(bV(t)), & V(t) \geq 0 \\ a_2 x(t) \sinh(bV(t)), & V(t) < 0 \end{cases} \quad (14)$$

$$\frac{dx}{dt} = g(V(t)) \cdot f(x(t)). \quad (15)$$

The second characteristic equation is mainly the state variable x with two functions responsible for controlling the operation, a threshold imposing factor and a boundary molding conditioning (15). The function $g(V(t))$ depicted in (16) introduces threshold voltages in the positive and negative regions V_p and V_n respectively, with no change allowable between these limiting points. Moreover, the rate of change beyond the set threshold is controlled by the variable A_p and A_n

$$g(V(t)) = \begin{cases} A_p (e^{V(t)} - e^{V_p}), & V(t) > V_p \\ -A_n (e^{-V(t)} - e^{V_n}), & V(t) < -V_n \\ 0, & -V_n \leq V(t) \leq V_p \end{cases} \quad (16)$$

$$dv_{p/n} = \underbrace{\alpha \cdot \theta (v_{p/n_0} - v_{p/n}) dt}_{\text{deterministic term}} + \underbrace{(V - \delta V - v_{p/n}) dN(\tau)}_{\text{stochastic term}}. \quad (17)$$

Incorporating the stochasticity into this model adds a lot of value to it as it is a prominent feature to have a reasonable level of variability in the operation of neuromorphic circuits [60], [61]. It allows for having an inherent noise feature embodied within a single circuit element that exhibits agility and integration over large scale systems. Equation (17) covers the mathematical form of the endorsed stochasticity on the positive and negative thresholds. From the modeling perspective, tackling the stochasticity application in this model requires a scaling to the parameter α_0 as a response to the threshold voltage modification according to the fit device. As the proposed fitting parameters are set based on the device description in [59] where the positive threshold voltage is set to 1.5 V, corresponding to three times smaller

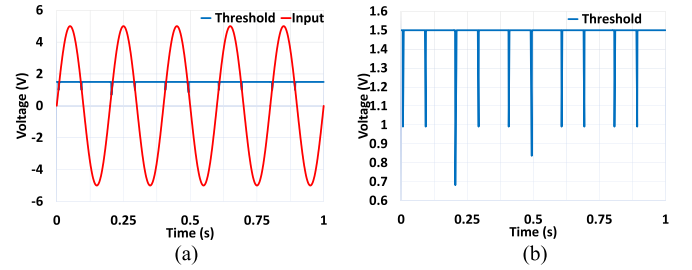


Fig. 12. *Analytical Model Threshold variability.* (a) Stochastic setting of the threshold voltage to reflect the non-deterministic internal operation of the device. (b) A finer resolution of the threshold variation over time.

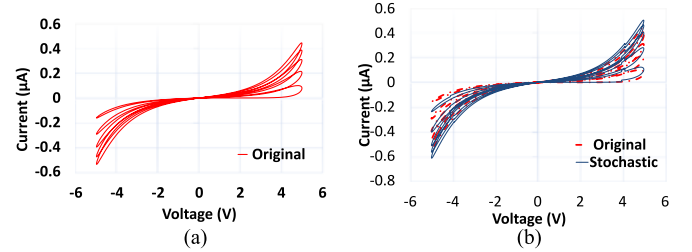


Fig. 13. *Analytical Stochastic Memristor Model.* (a) Deterministic output of the model parameters fit for the model in [59] for a sinusoidal input, $V_p = 1.5$ V, $V_n = 0.5$ V, $A_p = 0.005$, $A_n = 0.08$, $x_p = 0.2$, $x_n = 0.5$, $\alpha_p = 1.2$, $\alpha_n = 3$, $a_1 = 3.7(10^{-7})$, $a_2 = 4.35(10^{-7})$, $b = 0.7$, and $x_o = 0.1$. (b) Stochastic output with the same parameters with a modified intensity parameter α_0 to fit the positive and negative threshold accordingly.

than the original basis on which equation (5) was formulated. Similarly, the negative edge threshold was set to 0.5 V corresponding to around ten times smaller than the original values. This deviation from the adopted equation values was compensated by multiplying the threshold factor by the appropriate calibrating factor. As depicted in Fig. 12 the abrupt spikes in the threshold voltage was a direct consequence of the stochasticity application. It modifies the threshold of the device based on a probability of operation and switching. Furthermore, this variation was directly conveyed in the I - V relationship where the point of operation is divergent from the deterministic ones due to the induced non-determinism of the underlying behavior. Fig. 13(a) shows the original output response whereas (b) incorporates the stochasticity along with the original output.

C. Simmons Tunnel Barrier Model

An acutely fit model to the measurement and experimental data, the Pickett model [44] is a nonlinear representation of the bipolar switching. Its conductance change is based on a Simmons tunnel barrier width w that lies in series with an internal resistor cumulatively affecting the overall device characteristics. The applied current triggers the change of the state variable w with time due to its exponential effect on the velocity of the ionized dopants. This dependence leads to a nonsymmetrical ON and OFF switching dynamics with an ionic diffusion highly susceptible to the polarity of the input. The general equations portraying the behavior of this memristor model are rooted

back to the physical realizations attained for fabricated devices and fitted through an extensive regression analysis.

OFF switching ($i > 0$)

$$\frac{dw}{dt} = f_{\text{off}} \sinh\left(\frac{i}{i_{\text{off}}}\right) \exp\left[-\exp\left(\frac{w - a_{\text{off}}}{w_c} - \frac{|i|}{b}\right) - \frac{w}{w_c}\right]. \quad (18)$$

ON switching ($i < 0$)

$$\frac{dw}{dt} = f_{\text{on}} \sinh\left(\frac{i}{i_{\text{on}}}\right) \exp\left[-\exp\left(-\frac{w - a_{\text{on}}}{w_c} - \frac{|i|}{b}\right) - \frac{w}{w_c}\right]. \quad (19)$$

This current driven model has threshold values in the ON and OFF switching that act as a limiting factor for the change in the state, which is considered negligible below the assigned constraining boundaries. Moreover, the rate of change is tuned through the fitting parameters f_{on} and f_{off} , and the state variable x is confined within its set boundaries through the parameters a_{on} and a_{off} on both edges. The current-voltage relationship is not an explicit one but rather based on the Simmons tunneling model [62]

$$i = \frac{j_0 A}{(\Delta w)^2} \left(\phi_1 e^{-B\sqrt{\phi_1}} - (\phi_1 + e|v_g|) e^{-B\sqrt{\phi_1 + e|v_g|}} \right) \quad (20)$$

$$da_{\text{on/off}} = \underbrace{\alpha \cdot \theta(a_0 - a_{\text{on/off}}) dt}_{\text{deterministic term}} + \underbrace{(w - \delta w - a_0) dN(\tau)}_{\text{stochastic term}}. \quad (21)$$

The parameters in (20) are set in the spice model provided by Pickett [63] where a series resistance R_s of 215 Ω along with the tunnel barrier constitute the internal structure of the device and its corresponding state. The stochasticity in this case, is incorporated in a similar fashion to the prior models where the current threshold is the affected parameter. Equation (21) induces the stochastic dimension into the model with a variation set on the a parameter that governs the switching points of the model. On a finer scale with respect to the model fitting parameters, the equation for the variability is adjusted by a multiplication of the instantaneous resistance and the input current to account for the respective probability of switching below the set current limits. Considering the difference in the negative and positive thresholds, the probabilities are also fit to account for the polarity impact. That is the Set/Reset regions are both induced with stochasticity factors adjusted accordingly. In a form of a reversed status of the I - V relationship, the Simmons tunnel barrier model has threshold currents in the range of μA . Thus, the instantaneous modification of threshold is not easily conveyed in the hysteresis figure. Its primary impact is basically in the values of the underlying resistance. However, holding the threshold voltage at the point of variation for an arbitrary period of time prior to resetting it to its original value, allows for this corresponding variability to be easily depicted in the hysteresis. This mechanism is shown in Fig. 14 with the threshold variation over the sinusoidal input. Moreover, the direct impact of this variability on the threshold is an added hysteresis modification that reflects the underlying setting. Fig. 15(a) and (b) shows the deterministic and stochastic behavior of the model, respectively. The internal kinetics are smooth and slow resulting in a minor variation in the location of the switching point with conservation

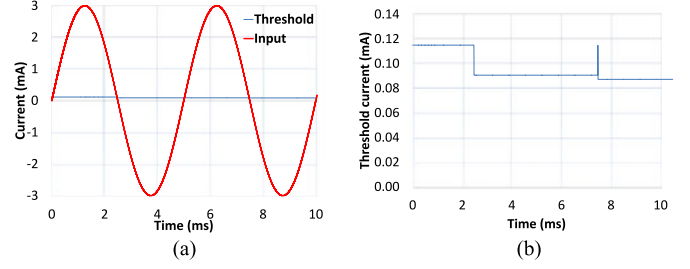


Fig. 14. *Simmons Tunnel Barrier Model.* (a) The variation of the threshold current as a response to an applied current input with incorporated stochasticity. (b) The threshold values with a finer resolution on the variation over time.

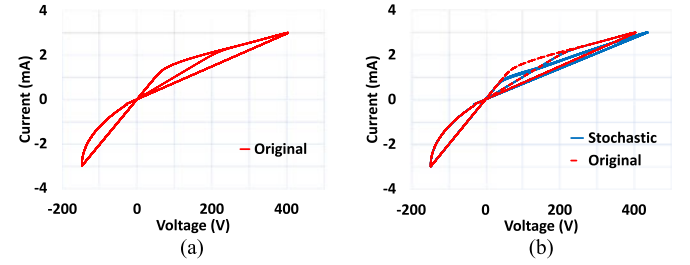


Fig. 15. *Tunnel Barrier Model Stochastic Hysteresis.* (a) Deterministic output of the model parameters for a sinusoidal input, $i_{\text{off}} = 115 \mu\text{A}$, $i_{\text{on}} = 8.9 \mu\text{A}$, $a_{\text{on}} = 2e-9$, $a_{\text{off}} = 1.2e-9$, $f_{\text{on}} = 40e-6$, $f_{\text{off}} = 3.5e-6$, $b = 500e-6$, $w_c = 107e-12$, $D = 3e-9$, $R_{\text{on}} = 100 \omega$, $R_{\text{off}} = 20 k\omega$. (b) Stochastic output with the same parameters with a modified intensity parameter α_0 to fit the positive and negative threshold accordingly.

of the overall system mechanism in terms of the speed of operation and dynamics. Table II summarizes the memristor models covered and the parameter affected by the stochasticity.

IV. APPLICATIONS

The characteristic features of the memristor have allowed for its integration into a broad set of applications including both analog and digital alike. Whether in IC design [19], [64], neuromorphics [65], [66], memory [67], [68] and digital applications [69], [70], [71]. Most implementations are prone to a factor of noise [72]; some actually use this parameter rather than combating it to help in improving the system performance. On the other hand, while others, particularly digital applications, tend to have stringent settings where the level of adherence to the original functionality provides a measure of robustness and repeatability conditions. Thus, the memristor innate stochasticity could be utilized as an alternative to noise injection in circuits where such behavior is beneficial in nature. It accommodates novelties in the design paradigm mapping to the stochastic electronics class of operation. It accounts for the inherent variability of the device kinetics, particularly the threshold and switching parameters to account for the variation required to randomize the noise effect and the consequent operation. On the other hand, digital applications tend to be more deterministic, and any shift from the expected output would overly change the circuit behavior or corresponding functionality. Two applications in the neuromorphic field and digital logic show contrasting views in terms of the use of the stochastic memristor within its design circuits.

TABLE II
MEMRISTOR MODELS WITH STOCHASTICITY INCORPORATED

| Model | State Equation | Stochastic Variable |
|-----------------------------------|---|---|
| Bipolar Memristor Model [56] | $\frac{dX}{dt} = f(V_M)[\theta(V_M)\theta(R_{\text{off}} - X) + \theta(-V_M)\theta(X - R_{\text{on}})]$ $f(V_M) = \beta V_M - 0.5\beta[V_M + V_t - V_M - V_t]$ $\frac{dx}{dt} = g(V(t)) \cdot f(x(t))$ | Threshold Voltage V_t |
| Analytical Memristor Model [58] | $g(V(t)) = \begin{cases} A_p(e^{V(t)} - e^{V_p}), & V(t) > V_p \\ -A_n(e^{-V(t)} - e^{V_n}), & V(t) < -V_n \\ 0, & -V_n \leq V(t) \leq V_p \end{cases}$ | Threshold voltages V_p and V_n |
| Simmons Tunnel Barrier Model [44] | $\frac{dw}{dt} = f_{\text{off}} \sinh\left(\frac{i}{i_{\text{off}}}\right) \exp\left[-\exp\left(\frac{w - a_{\text{off}}}{w_c} - \frac{ i }{b}\right) - \frac{w}{w_c}\right]$ $\frac{dw}{dt} = f_{\text{on}} \sinh\left(\frac{i}{i_{\text{on}}}\right) \exp\left[-\exp\left(-\frac{w - a_{\text{on}}}{w_c} - \frac{ i }{b}\right) - \frac{w}{w_c}\right]$ | Threshold parameters a_{off} and a_{on} |

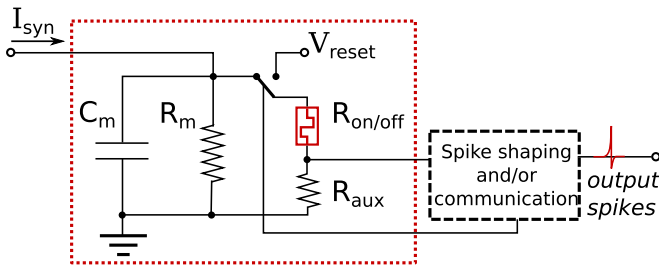


Fig. 16. Memristor based Neuron Circuit. The memristor is integrated into the block of the neuron circuit. It randomizes the spiking instants due to the switching threshold level variation

A. Neuromorphic Circuits

Neuromorphic circuits are hardware implementations that tend to convey the fundamental operational principles of neural systems [73]. Its principal components are comprised of neurons and synapses that are designed to capture the fundamental spiking behavior. A simple model widely used in the research community is the Integrate and Fire neuron (I&F) [74]. It builds upon simplifying the overall neuron operation to an integration of input charges, comparing with a set threshold, and consequently spikes generation once the integrated voltage exceeds the threshold. In its deterministic form, the I&F neuron serves as a good approximation to the nervous system dynamics. However, biological microcircuits are stochastic in nature and recent studies in neuroscience have supported the benefits and enhanced efficiency of injected noise in the process of learning and information processing [75]. Inducing stochasticity into the neuron takes on several forms, one of which is noise injection directly into the neuron [76]. It provides the versatility required for implementing stochastic spiking networks but at the expense of higher power dissipation and area measures.

Alternatively, and as a crucial component to the inherent stochasticity of the neuron operation, the memristor was integrated within the internal circuit of the I&F neuron model. It acted as a stochastic comparator where the threshold of the device would vary depending on a relationship binding the voltage application time and amplitude. Fig. 16 depicts the neuron circuit with the memristor set at the last stage prior to the spike

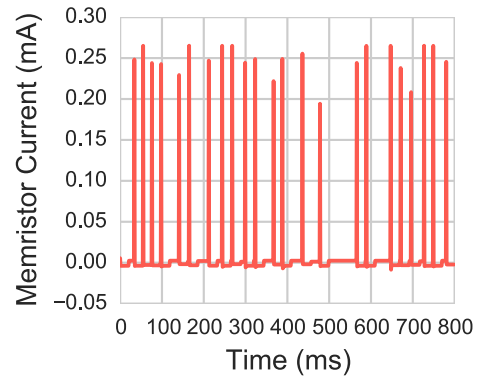


Fig. 17. Spiking Output Behavior. The spiking instants are random, providing a closer behavior to the biological systems and aiding in the learning and information processing mechanisms.

shaping block. With the incoming voltage, the memristor would behave in a stochastic manner, switching between high and low states, and consequently providing a variation in the output current levels. The voltage input to the spike shaping circuit was extracted from the auxiliary resistor connected in series with the memristor. Thus, the spiking instants were randomized through the variation of the threshold level mimicking the behavior of an added noise to the input current. This inherent variable threshold molded the spiking instants and the overall system behavior.

The resultant switching characteristics shaped the random spiking sequences to an extent akin to the biological neurons responses as shown in Fig. 17. The incorporation of the memristor in the circuit of this neuromorphic architecture represents a novel depiction of the circuit with enhancements in the area and power dissipation metrics of the design [18]. This implementation served to show the efficiency of the stochasticity of the memristor in providing an enhanced design. It aided in providing scalability and compactness, the commonly desired features, in very large scale integration circuits of the mind.

B. IMPLY Logic Application

In its abstract form, bipolar memristors could be seen as ideal switches and consequently used in the design of logic

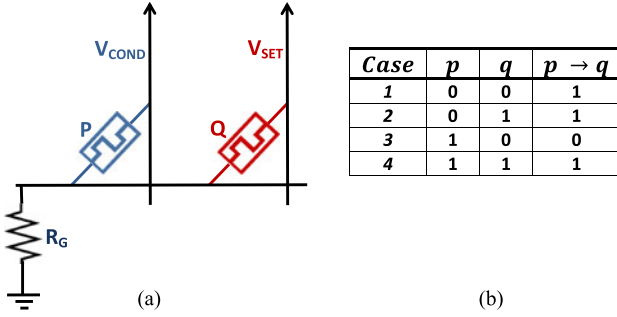


Fig. 18. *IMPLY Logic*. (a) Imply logic circuit utilizing the memristors as abstract switches top perform the *imply* (\Rightarrow) operation [77]. (b) The truth table for the 2-input *imply* operation.

operations. It could hold one of the two states, high resistance noted by R_{off} or what corresponds to a logic 0 and low resistance state R_{on} corresponding to logic 1. Investigating the applicability of the stochastic memristor within the digital logic applications aims to provide a preliminary overview of the underlying risks and functionality issues encountered. Thus, the functionality of the *imply* (\Rightarrow) operator is considered with the corresponding circuit implications addressed in regards to the induced stochasticity.

The basic operation principle of the *imply* operator lies in the conditional switching of a secondary memristor in response to the state of the primary one. Fig. 18(a) depicts the underlying circuit for this digital application. The two memristors, primary (p) and secondary (q), are separately connected to tri-state voltage drivers at one end and to a common resistor R_G at the other end [77], [78]. The imply operation is based on a change of the state of the output, which is the secondary memristor q , once the primary memristor is in the low state and with the application of a toggling voltage of V_{COND} smaller than the switching threshold, the state of the memristor is preserved, whereas the secondary memristor, or the output, is set since the voltage drop across its terminal is sufficient to switch it into the ON state. The truth table for the operation highlighting the different cases for the inputs and the corresponding output is illustrated in Fig. 18(b).

Experimental verification of operation performed in [77] tests the complete set of cases illustrated in the truth table. However, once incorporating the stochasticity of the memristor, a radical shift is applied to the overall concept of operation. The conditional voltage that was ensuring a stable resistance across the primary memristor is no longer certain. On the contrary, stochastic switching would be responsible for changing the state of the p -memristor and consequently affecting the subsequent output state of the memristor q . The effect of stochasticity is seen where the p memristor is in the *OFF* state. Thoroughly investigating the first combination of the *IMPLY* truth table, with both inputs in the open state, the primary memristor p along with the secondary memristor q are set to 0. Fig. 19 shows a SPICE simulation of the deterministic use of the memristor within the *IMPLY* operator. As anticipated, the output was shifted into the *ON* state due to the combination of the toggling pulses applied at the input. However, once the weak programming conditions

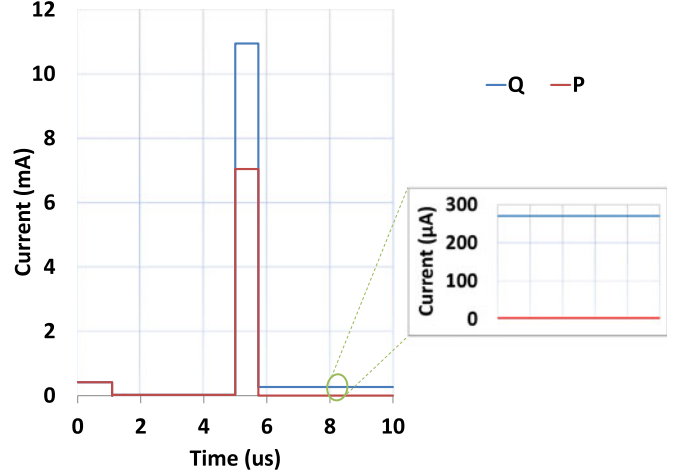


Fig. 19. *Deterministic IMPLY Output*. The particular output of case 1 in the truth table with both inputs sets to 0.

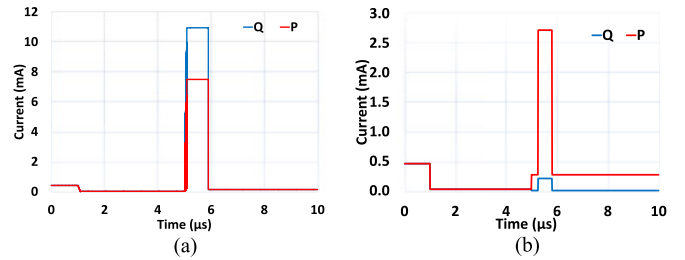


Fig. 20. *Stochastic ImPLY*. (a) Setting of both inputs p and q as a result of the endorsed stochasticity. (b) The output result of an *OFF* state for p and q is inverted due to the stochastic behavior of the memristors.

are active, the behavior of the logic circuit is compromised. As depicted in Fig. 20(a) the toggling pulse was sufficient to switch the output memristor into the *ON* state, but also managed to switch the input into the *ON* state as well resulting in a destructive setting. Moreover, a more severe situation would be in the case of the fast switching event of the primary memristor p and consequently blocking the output from going into the *SET* state. The result of such case is shown in Fig. 20(b) as another possible outcome of the induced stochasticity that could diminish the basic operation principles of the logic operator. Stochasticity of the memristor falsifies the expected digital behavior and the overall functionality of the logic operator. It jeopardizes the feasibility of the memristor functionality within the design schemes of digital gates. A simple application in a basic *IMPLY* circuit signifies the importance of robustness and consistency in the logic outputs. It further elaborates on the added caution required once dealing with non-linear devices and its underlying non-deterministic response. Nonetheless, it is noteworthy to mention that the memristor feasibility in the digital domain is not destructive in all aspects. Its use within the stochastic computing domain [79] is yet another proof of the huge potential ahead for the memristor in analog and digital applications alike.

V. CONCLUSION

A study of stochasticity induced into a range of threshold-based models for the memristor was presented. It provides a

quantification of the variability in the formation of the CF, and consequently in the switching characteristic between the two resistance extremities. A circuit simulator compatible model was provided, and its corresponding integration to various established models have produced stochastic hysteresis outputs. Its internal fitting parameters are adjusted accordingly for the switching probabilities to account for the threshold and operating parameters set for the specified device models. Model verification in terms of the distribution fitting and mapping to the original experimentally-extracted device characteristics signify the accuracy and validity of the proposed model. Furthermore, the utilization of the memristor in analog and digital applications provide contrasting views in terms of the enhancements of the performance metrics or jeopardizing the original operation.

ACKNOWLEDGMENT

The authors would like to thank G. Cauwenberghs, E. Neftci, and M. A. Zidan for helpful discussions and advice, and also the anonymous reviewers whose comments and suggestions have helped in improving the quality of the manuscript.

APPENDIX

The complete Verilog-A code for the integration of the stochasticity into the memristor models is available at <http://sensors.kaust.edu.sa>

Algorithm 1 Verilog-A Stochasticity Model

```

if ( $V(tp, bn) > Vini$ ) // initialization
     $Vini = V(tp, bn)$ ;
     $count = 0$ ; //restart count, increasing volt.
end
else if ( $V(tp, bn) \leq Vini$ ) begin
     $Vini = V(tp, bn)$ ;
     $count = count + 1$ ; //Decreasing voltage
end
 $\tau = pow(10, (-a * abs(Vm) + e))$ ; // mean time
if ( $dist\_f == 1$ ) begin
     $\lambda = 1/\tau$ ; // switching cst (Poisson)
     $prob\_t = \lambda * time\_step$ ; // instant. prb.
end else if ( $dist\_f == 2$ ) begin // Log-normal
     $prob\_t = (time\_step/\tau) * (exp(-pow(\sigma, 2)/2))$ ;
end
     $randm\_p = abs(\$rdist\_uniform(seed, 0, 1))$ ;
if ( $prob\_t \geq randm\_p$ ) begin
    if ( $(Vm > 0) \&\& (Vm < Vto)$ ) begin
         $Vt = Vm$ ; //positive switching point
    end
    else if ( $(Vm < 0) \&\& (abs(Vm) < Vto)$ ) begin
         $Vt = Vm$ ; //negative switching point
    end
end
else if ( $prob\_t < randm\_p$ ) begin
     $Vt = Vto$ ;
end

```

REFERENCES

- [1] T. J. Hamilton, S. Afshar, A. van Schaik, and J. Tapson, "Stochastic electronics: A neuro-inspired design paradigm for integrated circuits," *Proc. IEEE*, vol. 102, no. 5, pp. 843–859, May 2014.
- [2] M. Di Ventra, *Electrical Transport in Nanoscale Systems*. Cambridge, U.K.: Cambridge Univ. Press, 2008.
- [3] R. K. C. III, P. Lugli, and V. V. Zhirmov, "Science and engineering beyond Moore's law," *Proc. IEEE*, vol. 100, no. Centennial Issue, pp. 1720–1749, May 2012.
- [4] R. G. Dreslinski, M. Wiecekowsi, D. Blaauw, D. Sylvester, and T. Mudge, "Near-threshold computing: Reclaiming Moore's law through energy efficient integrated circuits," *Proc. IEEE*, vol. 98, no. 2, pp. 253–266, Feb. 2010.
- [5] A. F. Vincent, J. Larroque, N. Locatelli, N. Ben Romdhane, O. Bichler, C. Gamrat, W. S. Zhao, J.-O. Klein, S. Galdin-Retailleau, and D. Querlioz, "Spin-transfer torque magnetic memory as a stochastic memristive synapse for neuromorphic systems," *IEEE Trans. Biomed. Circuits Syst.*, vol. 9, no. 2, pp. 166–174, Apr. 2015.
- [6] B. Rajendran, M. Breitwisch, M.-H. Lee, G. W. Burr, Y.-H. Shih, R. Cheek, A. Schrott, C.-F. Chen, E. Joseph, R. Dasaka, H.-L. Lung, and L. Chung, "Dynamic resistance—A metric for variability characterization of phase-change memory," *IEEE Electron Device Lett.*, vol. 30, no. 2, pp. 126–129, Feb. 2009.
- [7] M. Suri, D. Querlioz, O. Bichler, G. Palma, E. Vianello, D. Vuillaume, C. Gamrat, and B. DeSalvo, "Bio-inspired stochastic computing using binary cbram synapses," *IEEE Trans. Electron Devices.*, vol. 60, no. 7, pp. 2402–2409, Jul. 2013.
- [8] P. Knag, W. Lu, and Z. Zhang, "A native stochastic computing architecture enabled by memristors," *IEEE Trans. Nanotechnol.*, vol. 13, no. 2, pp. 283–293, Mar. 2014.
- [9] A. Subramaniam, K. D. Cantley, G. Bersuker, D. Gilmer, and E. M. Vogel, "Spike-timing-dependent plasticity using biologically realistic action potentials and low-temperature materials," *IEEE Trans. Nanotechnol.*, vol. 12, no. 3, pp. 450–459, May 2013.
- [10] K. D. Cantley, A. Subramaniam, H. J. Stiegler, R. A. Chapman, and E. M. Vogel, "Hebbian learning in spiking neural networks with nanocrystalline silicon tfts and memristive synapses," *IEEE Trans. Nanotechnol.*, vol. 10, no. 5, pp. 1066–1073, Sep. 2011.
- [11] M. T. Ghoneim, M. A. Zidan, K. N. Salama, and M. M. Hussain, "Towards neuromorphic electronics: Memristors on foldable silicon fabric," *Microelectron. J.*, vol. 45, no. 11, pp. 1392–1395, 2014.
- [12] K.-H. Kim, S. Gaba, D. Wheeler, J. M. Cruz-Albrecht, T. Hussain, N. Srinivasa, and W. Lu, "A functional hybrid memristor crossbar-array/CMOS system for data storage and neuromorphic applications," *Nano Lett.*, vol. 12, no. 1, pp. 389–395, 2011.
- [13] A. Ascoli, F. Corinto, M. Gilli, and R. Tetzlaff, "Memristor for neuromorphic applications: Models and circuit implementations," in *Memristors and Memristive Systems*. New York, NY, USA: Springer-Verlag, 2014, pp. 379–403.
- [14] D. Kuzum, S. Yu, and H. S. P. Wong, "Synaptic electronics: Materials, devices and applications," *Nanotechnology*, vol. 24, no. 38, Sep. 2013.
- [15] M. Al-Shedivat, R. Naous, G. Cauwenberghs, and K. N. Salama, "Memristors empower spiking neurons with stochasticity," *IEEE J. Emerging Sel. Topics Circuits Syst.*, vol. 5, no. 2, pp. 242–253, Jun. 2015.
- [16] S. Shin, K. Kim, and S.-M. S. Kang, "Memristor macromodel and its application to neuronal spike generation," in *Proc. Eur. Conf. Circuit Theory Des.*, 2013, pp. 1–4.
- [17] M. Pickett, G. Medeiros-Ribeiro, and R. Williams, "A scalable neuristor built with Mott memristors," *Nature Mater.*, vol. 12, no. 2, pp. 114–117, 2013.
- [18] M. Al-Shedivat, R. Naous, E. Neftci, G. Cauwenberghs, and K. N. Salama, "Inherently stochastic spiking neurons for probabilistic neural computation," in *Proc. IEEE/EMBS 7th Int. Conf. Neural Eng.*, 2015, pp. 356–359.
- [19] M. A. Zidan, H. Omran, C. Smith, A. Syed, A. G. Radwan, and K. N. Salama, "A family of memristor-based reactance-less oscillators," *Int. J. Circuit Theory Appl.*, vol. 42, no. 11, pp. 1103–1122, 2014.
- [20] R. Waser and M. Aono, "Nanoionics-based resistive switching memories," *Nature Mater.*, vol. 6, no. 11, pp. 833–840, 2007.
- [21] T. Prodromakis, K. Michelakisy, and C. Toumazou, "Fabrication and electrical characteristics of memristors with tio_2/tio_{2+x} active layers," in *Proc. IEEE Int. Symp. Circuits Syst.*, 2010, pp. 1520–1522.

- [22] D. B. Strukov, G. S. Snider, D. R. Stewart, and R. S. Williams, "The missing memristor found," *Nature*, vol. 453, no. 7191, pp. 80–83, 2008.
- [23] S. Kvaterny, E. G. Friedman, A. Kolodny, and U. C. Weiser, "Team: Threshold adaptive memristor model," *IEEE Trans. Circuits Syst. I, Reg. Papers.*, vol. 60, no. 1, pp. 211–221, Jan. 2013.
- [24] H.-S. Wong, H.-Y. Lee, S. Yu, Y.-S. Chen, Y. Wu, P.-S. Chen, B. Lee, F. T. Chen, and M.-J. Tsai, "Metal-oxide RRAM," *Proc. IEEE*, vol. 100, no. 6, pp. 1951–1970, Jun. 2012.
- [25] D. B. Strukov and R. S. Williams, "Exponential ionic drift: Fast switching and low volatility of thin-film memristors," *Appl. Phys. A*, vol. 94, no. 3, pp. 515–519, 2009.
- [26] T. Prodromakis, B. P. Peh, C. Papavassiliou, and C. Toumazou, "A versatile memristor model with nonlinear dopant kinetics," *IEEE Trans. Electron Devices*, vol. 58, no. 9, pp. 3099–3105, Sep. 2011.
- [27] D. B. Strukov, J. L. Borghetti, and R. S. Williams, "Coupled ionic and electronic transport model of thin-film semiconductor memristive behavior," *Small*, vol. 5, no. 9, pp. 1058–1063, 2009.
- [28] Y. V. Pershin, S. La Fontaine, and M. Di Ventra, "Memristive model of amoeba learning," *Phys. Rev. E*, vol. 80, no. 2, p. 021926, 2009.
- [29] A. G. Radwan, M. A. Zidan, and K. Salama, "On the mathematical modeling of memristors," in *Proc. IEEE Int. Conf. Microelectron.*, 2010, pp. 284–287.
- [30] F. Corinto and A. Ascoli, "A boundary condition-based approach to the modeling of memristor nanostructures," *IEEE Trans. Circuits Systems I, Reg. Papers.*, vol. 59, no. 11, pp. 2713–2726, Nov. 2012.
- [31] Z. Biolek, D. Biolek, and V. Biolkova, "Spice model of memristor with nonlinear dopant drift," *Radioengineering*, vol. 18, no. 2, pp. 210–214, 2009.
- [32] S. H. Jo, K.-H. Kim, and W. Lu, "Programmable resistance switching in nanoscale two-terminal devices," *Nano Lett.*, vol. 9, no. 1, pp. 496–500, 2008.
- [33] Q. Li, A. Khiat, I. Salaoru, H. Xu, and T. Prodromakis, "Stochastic switching of tio₂-based memristive devices with identical initial memory states," *Nanoscale Res. Lett.*, vol. 9, no. 1, pp. 1–5, 2014.
- [34] A. Lacaita, A. Redaelli, D. Ielmini, F. Pellizzer, A. Pirovano, R. Bez, "Electrothermal and phase-change dynamics in chalcogenide-based memories," in *Proc. IEEE Int. Electron Devices Meet.*, 2004, pp. 911–914.
- [35] S. Yu, X. Guan, and H.-S. P. Wong, "On the stochastic nature of resistive switching in metal oxide RRAM: Physical modeling, Monte Carlo simulation, and experimental characterization," in *Proc. IEEE Int. Electron Devices Meet.*, 2011, pp. 17.3.1–17.3.4.
- [36] I. Salaoru, A. Khiat, Q. Li, R. Berdan, C. Papavassiliou, and T. Prodromakis, "Origin of the off state variability in ReRAM cells," *J. Phys. D, Appl. Phys.*, vol. 47, no. 14, p. 145102, 2014.
- [37] S. Menzel and R. Waser, "Analytical analysis of the generic set and reset characteristics of electrochemical metallization memory cells," *Nanoscale*, vol. 5, no. 22, pp. 11 003–11 010, 2013.
- [38] D. Ielmini, C. Cagli, and F. Nardi, "Resistance transition in metal oxides induced by electronic threshold switching," *Appl. Phys. Lett.*, vol. 94, no. 6, p. 063511, 2009.
- [39] D. Ielmini, "Modeling the universal set/reset characteristics of bipolar RRAM by field- and temperature-driven filament growth," *IEEE Trans. Electron Devices*, vol. 58, no. 12, pp. 4309–4317, Dec. 2011.
- [40] X. Guan, S. Yu, H.-S. Wong, "A spice compact model of metal oxide resistive switching memory with variations," *IEEE Electron Device Lett.*, vol. 33, no. 10, pp. 1405–1407, Oct. 2012.
- [41] S. Ambrogio, S. Balatti, A. Cubeta, A. Calderoni, N. Ramaswamy, and D. Ielmini, "Statistical fluctuations in FfOx resistive-switching memory: Part I—Set/reset variability," *IEEE Trans. Electron Devices*, vol. 61, no. 8, pp. 2912–2919, Aug. 2014.
- [42] G. Medeiros-Ribeiro, F. Perner, R. Carter, H. Abdalla, M. D. Pickett, and R. S. Williams, "Lognormal switching times for titanium dioxide bipolar memristors: Origin and resolution," *Nanotechnology*, vol. 22, no. 9, p. 095702, 2011.
- [43] Y. Yang and W. Lu, "Nanoscale resistive switching devices: mechanisms and modeling," *Nanoscale*, vol. 5, no. 21, pp. 10 076–10 092, 2013.
- [44] M. D. Pickett, D. B. Strukov, J. L. Borghetti, J. J. Yang, G. S. Snider, D. R. Stewart, and R. S. Williams, "Switching dynamics in titanium dioxide memristive devices," *J. Appl. Phys.*, vol. 106, no. 7, p. 074508, 2009.
- [45] E. L. Crow and K. Shimizu, *Lognormal Distributions: Theory and Applications*, vol. 88. New York, NY, USA: Marcel Dekker, 1988.
- [46] L. O. Chua and S. M. Kang, "Memristive devices and systems," *Proc. IEEE*, vol. 64, no. 2, pp. 209–223, Feb. 1976.
- [47] A. Ascoli, F. Corinto, V. Senger, and R. Tetzlaff, "Memristor model comparison," *IEEE Circuits Syst. Mag.*, vol. 13, no. 2, pp. 89–105, Apr.–Jun. 2013.
- [48] K. Eshraghian, O. Kavehei, K.-R. Cho, J. M. Chappell, A. Iqbal, S. F. Al-Sarawi, and D. Abbott, "Memristive device fundamentals and modeling: Applications to circuits and systems simulation," *Proc. IEEE*, vol. 100, no. 6, pp. 1991–2007, Jun. 2012.
- [49] I. Vourkas, A. Batsos, and G. C. Sirakoulis, "Spice modeling of nonlinear memristive behavior," *Int. J. Circuit Theory Appl.*, vol. 43, pp. 553–565, 2015.
- [50] A. G. Radwan, M. A. Zidan, and K. Salama, "Hp memristor mathematical model for periodic signals and dc," in *Proc. IEEE 53rd Int. Midwest Symp. Circuits Syst.*, 2010, pp. 861–864.
- [51] A. Ascoli, R. Tetzlaff, F. Corinto, and M. Gilli, "Pspice switch-based versatile memristor model," in *Proc. IEEE Int. Symp. Circuits Syst.*, 2013, pp. 205–208.
- [52] J. Valsa, D. Biolek, and Z. Biolek, "An analogue model of the memristor," *Int. J. Numerical Model., Electron. Netw., Devices Fields*, vol. 24, no. 4, pp. 400–408, 2011.
- [53] D. Batas and H. Fiedler, "A memristor spice implementation and a new approach for magnetic flux-controlled memristor modeling," *Nanotechnology, IEEE Trans. Nanotechnol.*, vol. 10, no. 2, pp. 250–255, Mar. 2011.
- [54] K. Xu, Y. Zhang, L. Wang, M. Q. Yuan, Y. Fan, W. T. Joines, and Q. H. Liu, "Two memristor spice models and their applications in microwave devices," *IEEE Trans. Nanotechnol.*, vol. 13, no. 3, pp. 607–616, May 2014.
- [55] O. Kavehei, S. Al-Sarawi, K.-R. Cho, K. Eshraghian, and D. Abbott, "An analytical approach for memristive nanoarchitectures," *IEEE Trans. Nanotechnol.*, vol. 11, no. 2, pp. 374–385, Mar. 2012.
- [56] Y. V. Pershin, and M. Di Ventra, "Spice model of memristive devices with threshold," *Radioengineering*, vol. 22, no. 2, pp. 485–489, 2013.
- [57] D. Biolek, M. Di Ventra, and Y. V. Pershin, "Reliable spice simulations of memristors, memcapacitors and meminductors," *Radioengineering*, vol. 22, 2013.
- [58] C. Yakopcic, T. M. Taha, G. Subramanyam, R. E. Pino, and S. Rogers, "A memristor device model," *IEEE Electron Device Lett.*, vol. 32, no. 10, pp. 1436–1438, Oct. 2011.
- [59] T. Chang, S.-H. Jo, K.-H. Kim, P. Sheridan, S. Gaba, and W. Lu, "Synaptic behaviors and modeling of a metal oxide memristive device," *Appl. Phys. A*, vol. 102, no. 4, pp. 857–863, 2011.
- [60] J. Bill and R. Legenstein, "A compound memristive synapse model for statistical learning through STDP in spiking neural networks," *Front. Neurosci.*, vol. 8, 2014.
- [61] S. Yu, B. Gao, Z. Fang, H. Yu, J. Kang, and H.-S. P. Wong, "Stochastic learning in oxide binary synaptic device for neuromorphic computing," *Front. Neurosci.*, vol. 7, 2013.
- [62] J. G. Simmons, "Generalized formula for the electric tunnel effect between similar electrodes separated by a thin insulating film," *J. Appl. Phys.*, vol. 34, no. 6, pp. 1793–1803, 1963.
- [63] H. Abdalla and M. D. Pickett, "Spice modeling of memristors," in *Proc. IEEE Int. Symp. Circuits Syst.*, 2011, pp. 1832–1835.
- [64] S. Shin, K. Kim, and S. Kang, "Memristor applications for programmable analog ICs," *IEEE Trans. Nanotechnol.*, vol. 10, no. 2, pp. 266–274, Mar. 2011.
- [65] M. Hu, H. Li, Y. Chen, Q. Wu, G. S. Rose, and R. W. Linderman, "Memristor crossbar-based neuromorphic computing system: A case study," *IEEE Trans. Neural Netw. Learn. Syst.*, vol. 25, no. 10, pp. 1864–1878, Oct. 2014.
- [66] M. Soltiz, D. Kudithipudi, C. Merkel, G. S. Rose, and R. E. Pino, "Memristor-based neural logic blocks for nonlinearly separable functions," *IEEE Trans. Comput.*, vol. 62, no. 8, pp. 1597–1606, Aug. 2013.
- [67] M. A. Zidan, H. Omran, A. Sultan, H. Fahmy, and K. N. Salama, "Compensated readout for high-density MOS-gated memristor crossbar array," *IEEE Trans. Nanotechnol.*, vol. 14, no. 1, pp. 3–6, Jan. 2015.
- [68] M. A. Zidan, A. M. Eltawil, F. Kurdahi, H. A. Fahmy, and K. N. Salama, "Memristor multiport readout: A closed-form solution for sneak paths," *IEEE Trans. Nanotechnol.*, vol. 13, no. 2, pp. 274–282, Mar. 2014.
- [69] G. S. Rose, J. Rajendran, H. Manem, R. Karri, and R. E. Pino, "Leveraging memristive systems in the construction of digital logic circuits," *Proc. IEEE*, vol. 100, no. 6, pp. 2033–2049, Jun. 2012.
- [70] J. J. Yang, D. B. Strukov, and D. R. Stewart, "Memristive devices for computing," *Nature Nanotechnol.*, vol. 8, no. 1, pp. 13–24, 2013.
- [71] I. Vourkas and G. C. Sirakoulis, "A novel design and modeling paradigm for memristor-based crossbar circuits," *IEEE Trans. Nanotechnol.*, vol. 11, no. 6, pp. 1151–1159, Nov. 2012.
- [72] M. A. Zidan, H. A. H. Fahmy, M. M. Hussain, and K. N. Salama, "Memristor-based memory: The sneak paths problem and solutions," *Microwelectron. J.*, vol. 44, no. 2, pp. 176–183, 2013.

- [73] C. Mead and M. Ismail, *Analog VLSI Implementation of Neural Systems*. New York, NY, USA: Springer-Verlag, 1989.
- [74] G. Indiveri, B. Linares-Barranco, T. J. Hamilton, A. Van Schaik, R. Etienne-Cummings, T. Delbruck, S.-C. Liu, P. Dudek, P. Häfziger, S. Renaud *et al.*, "Neuromorphic silicon neuron circuits," *Frontiers Neurosci.*, vol. 5, 2011.
- [75] M. McDonnell and L. Ward, "The benefits of noise in neural systems: bridging theory and experiment," *Nature Rev. Neurosci.*, vol. 12, no. 7, pp. 415–426, 2011.
- [76] A. S. Cassidy, P. Merolla, J. V. Arthur, S. K. Esser, B. Jackson, R. Alvarez-icaza, P. Datta, J. Sawada, T. M. Wong, V. Feldman, A. Amir, D. B. Dayan Rubin, E. McQuinn, W. P. Risk, and D. S. Modha, "Cognitive computing building block: A versatile and efficient digital neuron model for neurosynaptic cores," presented at the Int. Joint Conf. Neural Networks, Dallas, TX, USA, 2013.
- [77] J. Borghetti, G. S. Snider, P. J. Kuekes, J. J. Yang, D. R. Stewart, and R. S. Williams, "Memristive switches enable stateful logic operations via material implication," *Nature*, vol. 464, no. 7290, pp. 873–876, 2010.
- [78] S. Kvatinsky, G. Satat, N. Wald, E. G. Friedman, A. Kolodny, and U. C. Weiser, "Memristor-based material implication (imply) logic: Design principles and methodologies," *IEEE Trans. Very Large Scale Integr. Syst.*, vol. 22, no. 10, pp. 2054–2066, Oct. 2014.
- [79] S. Gaba, P. Sheridan, J. Zhou, S. Choi, and W. Lu, "Stochastic memristive devices for computing and neuromorphic applications," *Nanoscale*, vol. 5, no. 13, pp. 5872–5878, 2013.



Rawan Naous (S'13) received the B.E. degree in electrical engineering from the American University of Beirut, Beirut, Lebanon, in 2005, and the M.Sc. degree in communications electronics (Hons.) from the Technical University of Munich (TUM), Munich, Germany, in 2007. She is currently working toward the Ph.D. degree in electrical engineering at the King Abdullah University of Science and Technology (KAUST), Thuwal, Saudi Arabia.

Prior to joining KAUST, she was a Lecturer of computer science and electrical engineering with

Prince Sultan University, Riyadh, Saudi Arabia, and Effat University, Jeddah, Saudi Arabia. Her current research interests include mixed analog–digital IC design, memristor, stochastic electronics, nonvolatile memory, neuromorphic system architecture, and embedded machine learning.



Maruan Al-Shedivat (S'14) received the B.S. degree in physics from Lomonosov Moscow State University, Moscow, Russia, the M.E. degree in data analysis from Yandex Data School, Moscow, in 2013, and the M.S. degree in computer science from the King Abdullah University of Science and Technology, Thuwal, Saudi Arabia, in 2015. He is currently working toward the Ph.D. degree at the School of Computer Science, Carnegie Mellon University, Pittsburgh, PA, USA.

His research interests mainly include machine learning, statistics, probabilistic models, information theory, and stochastic computation.



Khaled Nabil Salama (S'97–M'05–SM'10) received the B.S. degree (Hons.) from the Department of Electronics and Communications, Cairo University, Cairo, Egypt, in 1997, and the M.S. and Ph.D. degrees from the Department of Electrical Engineering, Stanford University, Stanford, CA, USA, in 2000 and 2005, respectively.

He was an Assistant Professor with Rensselaer Polytechnic Institute, Troy, NY, USA, between 2005 and 2009. He joined the King Abdullah University of Science and Technology, Thuwal Saudi Arabia, in January 2009 and was the founding Program Chair until August 2011. His work on CMOS sensors for molecular detection has been supported by the National Institutes of Health and the Defense Advanced Research Projects Agency, awarded the Stanford-Berkeley Innovators Challenge Award in Biological Sciences and was acquired by Lumina, Inc. He is an Author of 100 papers and eight patents on low-power mixed-signal circuits for intelligent fully integrated sensors and nonlinear electronics, especially memristor devices.